

# Microstructural effects on the flow law of power-law fluids through fibrous media

Z Idris<sup>1</sup>, L Orgéas<sup>1</sup>, C Geindreau<sup>1</sup>, J-F Bloch<sup>2</sup> and J-L Auriault<sup>1</sup>

<sup>1</sup> Laboratoire Sols-Solides-Structures (3S), CNRS - INPG - UJF, BP 53, 38041 Grenoble Cedex, France

<sup>2</sup> Laboratoire de Génie des Procédés Papetiers (LG2P), Ecole Française de Papeterie de Grenoble - INPG, 38000 Grenoble Cedex, France

E-mail: Laurent.Orgéas@hmg.inpg.fr

Received 19 March 2004

Published 9 August 2004

Online at [stacks.iop.org/MSMSE/12/995](http://stacks.iop.org/MSMSE/12/995)

doi:10.1088/0965-0393/12/5/016

## Abstract

In this work, the flow of power-law fluids through anisotropic fibrous media is revisited, upscaling the fluid flow at the pore scale with the homogenization method of multiple scale expansions for periodic structures. This upscaling technique permits a quantitative study of the seepage law by performing numerical simulation with simple two-dimensional periodic arrays of circular solid inclusions. The significant role of the solid fraction, the fluid rheology and the porous media anisotropy on the resulting macroscopic flow law is underlined from the simulation.

(Some figures in this article are in colour only in the electronic version)

## 1. Introduction

Fluid flow through anisotropic fibrous media plays an important role in many engineering applications, such as polymer composites, textiles and paper manufacturing processes. Thus, to optimize such processes, a proper description of the flow through such porous media is required.

When the flowing fluid can be considered as Newtonian, straightforward extensions of the well-known Darcy law [1] to anisotropic fibrous media permit a good prediction of the flow process. They are now widely used to optimize, for instance, paper pressing or composites manufacturing processes such as resin transfer moulding (RTM) [2]. Constitutive parameters that are required are the fluid viscosity and the components of the permeability tensor. In order to avoid cumbersome laboratory experiments, these components can be determined using analytical or numerical approaches. In the literature, there exist extensive theoretical and numerical works on the Stokes flow in periodic and random arrays of cylinders [3–19].

From these works, it is now well known that the permeability of such a porous medium depends on size, concentration and arrangement of fibres. These works, carried out on a particular geometry, represent an interesting step toward understanding the flow through more complex porous media as in [20].

In contrast, the modelling of the flow of non-Newtonian fluids through anisotropic fibrous media has received less attention, very few experimental, analytical or numerical studies are found in the literature. Most of them deal with power-law flowing fluid; this simple estimation of the fluid rheology is a first and reasonable approximation to model flow phenomena arising in many manufacturing processes such as paper or textile coating, and thermoplastics polymer composites processing [21,22]. Due to the strong coupling between the porous media geometry and the rheology of the fluid, the extension of the Darcy law to power-law fluid flowing in anisotropic porous media is quite tricky. Several authors have proposed quantitative analytical expressions of the flow law that are often restricted to simple fibrous media. They are generally one-dimensional modified versions of Darcy law built on phenomenological considerations or direct numerical simulation at the pore scale [23–27], except in the latest work of Woods *et al* [28, 29]. Indeed, Woods *et al* proposed a first complete expression of the flow law of a power-law fluid through a rectangular array of parallel and infinite cylinder of elliptic cross-section. However, the flow law given in [29] is not intrinsic, since it is not written in a tensorial form. Moreover, its extension to another type of fibrous media is not straightforward. On the other hand, recent theoretical investigations based on rigorous upscaling techniques have proposed the general structure and the fundamental properties of the flow law of power-law fluids through fibrous media [30–32]. In particular, Auriault *et al* [32] have derived the most general tensorial form of the flow law in systems of different types of anisotropy. Unfortunately, no quantitative study was performed from these purely theoretical works to link the constitutive parameters of the macroscopic flow law with microstructural ones characterizing the fibrous media geometry at the pore scale, namely the rheology of the fluid.

Hence, the aim of this work is (i) to study quantitatively the flow of power-law fluids through anisotropic fibrous media following the general and theoretical framework proposed in [32], (ii) to emphasize the role of microstructural parameters on the resulting macroscopic flow law. For this purpose, a brief presentation of the upscaling technique used in [32], as well as the fundamental results deduced from it are given in section 2. In section 3, we investigate quantitatively the as-derived flow law. This is done by solving numerically, on representative elementary volumes of fibrous media, special boundary-value problems directly deduced from the upscaling process. In this paper, such a methodology is achieved in the case of two very simple types of anisotropic fibrous media, i.e. square or triangular arrays of infinite and parallel cylinders of circular cross-section. The choice of such simple microstructures is not a restriction of the present methodology. To validate our approach, we compare our results with analytical or numerical quantitative results reported in the literature. Conclusions drawn from this numerical work underline the significant role of the solid fraction, the fluid rheology, the porous media anisotropy on the resulting macroscopic flow law and the domain of validity of models already proposed in the literature.

## 2. Determination of the macroscopic flow law

In previous works [30–32], the flow law for a power-law fluid in porous media was rigorously derived by upscaling the physics at the pore scale. A deterministic upscaling technique was used, namely the homogenization method of multiple scale expansions for periodic structures [33–35]. Generally speaking, the main advantages of the method rely upon the possibility of: (a) avoiding prerequisites at the macroscopic scale; (b) modelling finite size

macroscopic samples; (c) modelling macroscopically non-homogeneous media or phenomena; (d) modelling problems with several separations of scales; (e) modelling several simultaneous phenomena; (f) determining whether the system ‘medium + phenomena’ can be homogenized or not; (g) providing the domains of validity of the macroscopic models. The objective of this section is to give a brief review of the derivation by homogenization of the flow law for a power-law fluid in porous media. For details related to the analysis below, the reader is referred to [32].

### 2.1. Upscaling process: methodology

Physical phenomena in heterogeneous systems such as porous media can be homogenized, i.e. may be modelled by an equivalent continuous macroscopic description, provided that the condition of separation of scales is satisfied [33, 34]. This fundamental condition may be expressed as

$$\varepsilon = \frac{l}{L} \ll 1, \quad (1)$$

in which  $l$  and  $L$  are the characteristic lengths of the heterogeneities at the pore scale and of the macroscopic sample or excitation, respectively. Based on the pore scale description of the problem (section 2.2) and assuming without loss of generality the periodicity of the medium, the macroscopic equivalent model is obtained from the description at the heterogeneity scale by [35]: (i) writing the local description in a dimensionless form and estimating the order of magnitude of the resulting dimensionless numbers with respect to the scale ratio  $\varepsilon$  (section 2.3); (ii) looking for the unknown fields in the form of asymptotic expansions in powers of  $\varepsilon$  and solving the boundary-value problems that arise at the successive orders of  $\varepsilon$ , after introducing the asymptotic expansions in the local dimensionless description (section 2.4). The macroscopic equivalent model is obtained from the compatibility conditions, which are the necessary conditions for the existence of the solutions to the boundary-value problems.

### 2.2. Fluid flow description at the pore scale

Consider the flow through a porous medium of periodic representative elementary volume (REV)  $\Omega$  and bounded by  $\partial\Omega$ . Within the periodic REV, the fluid occupies the domain  $\Omega_f$ , the solid occupies the domain  $\Omega_s$ , and the fluid–solid interface is denoted by  $\Gamma$  (figure 1). Thus, the solid fraction and the porosity of the porous medium are defined as  $c = \Omega_s/\Omega$  and  $\phi = \Omega_f/\Omega$ , respectively. The porous matrix is assumed to be rigid and the liquid is viewed as an incompressible and purely viscous fluid. Its stress tensor at the pore scale  $\boldsymbol{\sigma}$  is defined by the following constitutive equations:

$$\boldsymbol{\sigma} = -p\boldsymbol{\delta} + 2\mu\mathbf{D}, \quad (2)$$

where  $p$  is the pressure,  $\boldsymbol{\delta}$  is the identity tensor,  $\mu$  is the viscosity and  $\mathbf{D}$  is the strain rate tensor defined as a function of the local velocity field  $\mathbf{v}$ , i.e. the velocity field at the pore scale,

$$\mathbf{D} = \frac{1}{2}(\nabla\mathbf{v} + \nabla^T\mathbf{v}). \quad (3)$$

The fluid viscosity  $\mu$  is supposed to be a power-law function of the microscopic shear strain rate  $\dot{\gamma}_{\text{eq}}$ , i.e.

$$\mu = \mu_0\dot{\gamma}_{\text{eq}}^{n-1}, \quad \dot{\gamma}_{\text{eq}} = \sqrt{2\mathbf{D} : \mathbf{D}}, \quad (4)$$

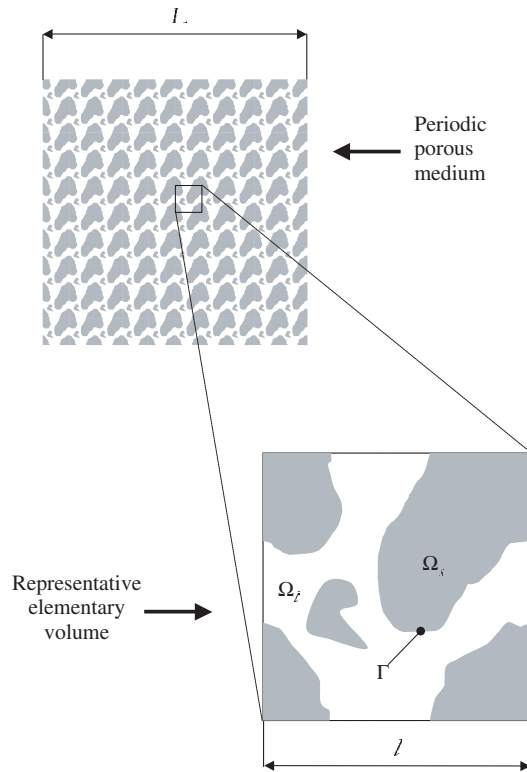


Figure 1. A schematic of the periodic porous medium and associated REV,  $\Omega$ .

where  $\mu_0$  is the shear consistency of the fluid, and where the power-law exponent  $n$  characterizes the strain rate sensitivity of the fluid. At the pore scale, the momentum balance for an isothermal steady slow flow (inertial effects are neglected) of such a power-law fluid is written as

$$2\mu_0 \nabla \cdot (\dot{\gamma}_{eq}^{n-1} \mathbf{D}) = \nabla p \quad \text{in } \Omega_i. \tag{5}$$

To complete the pore scale description, the incompressibility condition as well as the no-slip boundary condition on  $\Gamma$  have to be considered,

$$\nabla \cdot \mathbf{v} = 0 \quad \text{in } \Omega_i, \tag{6}$$

$$\mathbf{v} = 0 \quad \text{on } \Gamma. \tag{7}$$

The set of equations (5)–(7) is the pore scale description of the flow problem.

### 2.3. Dimensionless pore scale description

Let us introduce in equations (5)–(7) the following representation of all dimensional variables:

$$\mathbf{X} = l\mathbf{y}, \quad \mathbf{v} = v_c \mathbf{v}^*, \quad p = p_c p^*, \quad \mu_0 = \mu_0 \mu_0^*, \tag{8}$$

where the subscript ‘c’ and the superscript ‘\*’ denotes characteristic quantities (constant) and dimensionless variables, respectively. The vector  $\mathbf{X}$  is the physical space variable and  $\mathbf{y}$  the so-called dimensionless microscopic space variable [35]. It is obtained by normalizing  $\mathbf{X}$

using the local pore length scale  $l$ . The formal dimensionless set that describes the flow is thus written as

$$2\mu_0^* \nabla_{\mathbf{y}} \cdot (\dot{\gamma}_{\text{eq}}^{*(n-1)} \mathbf{D}^*) = Q^* \nabla_{\mathbf{y}} p^* \quad \text{in } \Omega_1^*, \tag{9}$$

$$\nabla_{\mathbf{y}} \cdot \mathbf{v}^* = 0 \quad \text{in } \Omega_1^*, \tag{10}$$

$$\mathbf{v}^* = 0 \quad \text{on } \Gamma^*, \tag{11}$$

where  $\nabla_{\mathbf{y}}$  is the dimensionless gradient operator with respect to the microscopic space variable  $\mathbf{y}$ . The dimensionless pore scale description (9)–(11) introduces a dimensionless number,  $Q^*$ , which represents the ratio of the pressure term to the viscous forces:

$$Q^* = \frac{p_c}{\mu_0} \left(\frac{l}{v_c}\right)^{n-1} \left(\frac{l}{L}\right). \tag{12}$$

The order of magnitude of  $Q^*$  was estimated using the following phenomenological argument: the local viscous flow is driven by a macroscopic pressure gradient [35], which is equivalent to

$$\frac{l}{\mu_0} \left(\frac{l}{v_c}\right)^{n-1} \left(\frac{l}{L}\right) = \mathcal{O}\left(\frac{p_c}{L}\right), \tag{13}$$

so that

$$Q^* = \frac{p_c}{\mu_0} \left(\frac{l}{v_c}\right)^{n-1} \left(\frac{l}{L}\right) = \mathcal{O}(\varepsilon^{-1}). \tag{14}$$

#### 2.4. Upscaling

We may now employ the homogenization procedure by first introducing the multiple scale coordinates [33, 34]; the macroscopic dimensionless space variable,  $\mathbf{x} = \mathbf{X}/L$  and the microscopic dimensionless space variable,  $\mathbf{y} = \mathbf{X}/l$ , both being linked by  $\mathbf{x} = \varepsilon \mathbf{y}$ . Applying the technique of multiple scale expansions, the velocity  $\mathbf{v}^*$  and the pressure  $p^*$  fields may be put in the form of asymptotic expansions of powers of  $\varepsilon$

$$\mathbf{v}^* = \mathbf{v}^{*(0)}(\mathbf{x}, \mathbf{y}) + \varepsilon \mathbf{v}^{*(1)}(\mathbf{x}, \mathbf{y}) + \varepsilon^2 \mathbf{v}^{*(2)}(\mathbf{x}, \mathbf{y}) + \dots, \tag{15}$$

$$p^* = p^{*(0)}(\mathbf{x}, \mathbf{y}) + \varepsilon p^{*(1)}(\mathbf{x}, \mathbf{y}) + \varepsilon^2 p^{*(2)}(\mathbf{x}, \mathbf{y}) + \dots, \tag{16}$$

where the velocity fields  $\mathbf{v}^{*(i)}(\mathbf{x}, \mathbf{y})$  and the pressure fields  $p^{*(i)}(\mathbf{x}, \mathbf{y})$  are  $\mathbf{y}$ -periodic. The dimensionless gradient operator is now written as  $\nabla_{\mathbf{y}} + \varepsilon \nabla_{\mathbf{x}}$ . Incorporating the above expansions in the dimensionless set (9)–(11) and identifying at the successive orders of  $\varepsilon$  allow the construction of appropriate boundary-value problems. Solving these boundary-value problem leads to the macroscopic description [32].

The lowest order yields

$$\nabla_{\mathbf{y}} p^{*(0)} = 0, \quad p^{(0)} = p^{*(0)}(\mathbf{x}). \tag{17}$$

Hence, the first-order pressure is constant over the period  $\Omega^*$ .

By considering the next order, a boundary-value problem with respect to the first order velocity  $\mathbf{v}^{*(0)}$  and to the second order pressure  $p^{*(1)}$  is obtained:

$$2\mu_0^* \nabla_{\mathbf{y}} \cdot \left( \left( \dot{\gamma}_{\text{eq}}^{*(0)} \right)^{n-1} \mathbf{D}^{*(0)} \right) = \nabla_{\mathbf{y}} p^{*(1)} + \nabla_{\mathbf{x}} p^{*(0)} \quad \text{in } \Omega_1^*, \tag{18}$$

$$\nabla_{\mathbf{y}} \cdot \mathbf{v}^{*(0)} = 0 \quad \text{in } \Omega_1^*, \tag{19}$$

$$\mathbf{v}^{*(0)} = 0 \quad \text{on } \Gamma^* \tag{20}$$

with

$$\mathbf{D}^{*(0)} = \frac{1}{2}(\nabla_y \mathbf{v}^{*(0)} + \nabla_y^T \mathbf{v}^{*(0)}), \quad \dot{\gamma}_{\text{eq}}^{*(0)} = \sqrt{2\mathbf{D}^{*(0)} : \mathbf{D}^{*(0)}}, \quad (21)$$

where  $\mathbf{v}^{*(0)}$  and  $p^{*(1)}$  are  $\mathbf{y}$ -periodic. The macroscopic gradient of pressure  $\nabla_x p^{*(0)}$  in (18) appears as a source term. A weak formulation of the above set of equations is required for determining its solution. For this purpose, we shall introduce the Hilbert space  $W^*$  of vectors  $\mathbf{u}^*$  of  $\Omega_1^*$ , that are  $\mathbf{y}$ -periodic, divergence free and zero-valued over  $\Gamma^*$ . This Hilbert space is equipped with the following inner product:

$$(\mathbf{u}^*, \mathbf{v}^*)_{W^*} = \int_{\Omega_1^*} \nabla_y \mathbf{u}^* : \nabla_y \mathbf{v}^* \, dy. \quad (22)$$

Let us now multiply equation (18) by  $\mathbf{u}^* \in W^*$  and integrate it over  $\Omega_1^*$ . Integrating by parts, applying the divergence theorem and then using the property of periodicity and the boundary condition on  $\Gamma^*$ , the following weak formulation is finally obtained:

$$\forall \mathbf{u}^* \in W^*, \quad \int_{\Omega_1^*} 2\mu_0^* (\dot{\gamma}_{\text{eq}}^{*(0)})^{n-1} \mathbf{D}^{*(0)} : \mathbf{D}^*(\mathbf{u}^*) \, dy = - \int_{\Omega_1^*} \mathbf{u}^* \cdot \nabla_x p^{*(0)} \, dy. \quad (23)$$

It can be shown that the above problem presents a unique solution [32]. Moreover, the weak form (23) shows that the fluid velocity  $\mathbf{v}^{*(0)}$  is a function of the microscopic space variable  $\mathbf{y}$ , the macroscopic gradient of pressure  $\nabla_x p^{*(0)}$ , the material properties of the fluid ( $\mu_0^*$  and  $n$ ), and the geometry of the porous medium:

$$\mathbf{v}^{*(0)}(\mathbf{x}, \mathbf{y}) = \mathbf{g}^*(\mathbf{y}, \nabla_x p^{*(0)}, \mu_0^*, n, \text{geometry}). \quad (24)$$

Finally, the integration of the volume balance at the second order,

$$\nabla_x \cdot \mathbf{v}^{*(0)} + \nabla_y \cdot \mathbf{v}^{*(1)} = 0 \quad \text{in } \Omega_1^*, \quad (25)$$

over  $\Omega_1^*$ , yields

$$\begin{aligned} \nabla_x \cdot \langle \mathbf{v}^{*(0)} \rangle &= 0 \quad \text{in } \Omega_1^*, \\ \langle \mathbf{v}^{*(0)} \rangle &= \frac{1}{\Omega^*} \int_{\Omega_1^*} \mathbf{v}^{*(0)} \, dy = \mathbf{G}^*(\nabla_x p^{*(0)}, \mu_0^*, n, \text{geometry}), \end{aligned} \quad (26)$$

which represents the dimensionless macroscopic equivalent behaviour within an order  $\mathcal{O}(\varepsilon)$  approximation. The second equality in (26) represents the dimensionless macroscopic flow law for power-law fluid in a given porous media.

## 2.5. Comments

The above derivation of macroscopic flow law for a power-law fluid in porous media conjures up the following comments:

- By definition, the macroscopic velocity  $\langle \mathbf{v}^{*(0)} \rangle$  is a volume average velocity. It can be shown that this volume average is equal to a surface average, which ascribes to  $\langle \mathbf{v}^{*(0)} \rangle$  the required properties of a Darcy's velocity [35].
- Equations (23) and (26) show that the macroscopic velocity  $\langle \mathbf{v}^{*(0)} \rangle$  is an homogeneous function of degree  $1/n$  of the macroscopic pressure  $\nabla_x p^{*(0)}$  [32]:

$$\forall \lambda \in \mathbb{R}, \quad \langle \mathbf{v}^{*(0)}(\lambda \nabla_x p^{*(0)}) \rangle = |\lambda|^{(1-n)/n} \lambda \langle \mathbf{v}^{*(0)}(\nabla_x p^{*(0)}) \rangle. \quad (27)$$

- When  $n = 1$ , equations (23) and (26) prove that  $\langle \mathbf{v}^{*(0)} \rangle$  is a linear function of  $\nabla_x p^{*(0)}$  [35].

(d) Finally, the dimensional flow law for a power-law fluid through a rigid porous media can be put in the form, within a relative error of  $\mathcal{O}(\varepsilon)$ ,

$$\langle \mathbf{v}^{(0)} \rangle = - \left( \frac{l^2}{\mu_0} \right)^{1/n} l^{(1-n)/n} \mathbf{H}(\nabla p^{(0)}) \tag{28}$$

or

$$\nabla p^{(0)} = - \frac{\mu_0}{l^2} \left[ \frac{1}{l} \right]^{n-1} \mathbf{F}(\langle \mathbf{v}^{(0)} \rangle) \tag{29}$$

with

$$\nabla \cdot \langle \mathbf{v}^{(0)} \rangle = 0, \tag{30}$$

where  $\mathbf{H}$  and  $\mathbf{F}$  are, respectively, homogeneous functions of degree  $1/n$  and  $n$  of the macroscopic gradient of pressure  $\nabla p^{(0)}$  and the velocity  $\langle \mathbf{v}^{(0)} \rangle$ .

2.6. Microstructural effects on the form of the macroscopic flow law

In [32], the most general tensorial form of the flow law in porous media of different types of anisotropy has been investigated. In this section, we briefly outline the role of the microstructure in the form of the flow law in the particular cases where the porous media exhibit isotropy or orthotropy.

2.6.1. Isotropy. In this case, the previous flow law can be put in the form,

$$\langle \mathbf{v}^{(0)} \rangle = - \left( \frac{k^* l^2}{\mu_0} \right)^{1/n} \left( \frac{\|\nabla p^{(0)}\|}{l} \right)^{(1-n)/n} \nabla p^{(0)} \tag{31}$$

or

$$\nabla p^{(0)} = - \frac{\mu_0}{k^* l^2} \left[ \frac{\|\langle \mathbf{v}^{(0)} \rangle\|}{l} \right]^{n-1} \langle \mathbf{v}^{(0)} \rangle, \tag{32}$$

where  $k^*$  is a dimensionless rheological function that may depend on  $n$  and on the geometry of the porous medium. In the particular case where  $n = 1$ , the above equations become

$$\langle \mathbf{v}^{(0)} \rangle = - \frac{l^2 k^*}{\mu_0} \nabla p^{(0)} \tag{33}$$

and

$$\nabla p^{(0)} = - \frac{\mu_0}{k^* l^2} \langle \mathbf{v}^{(0)} \rangle, \tag{34}$$

where  $k^*$  stands for the usual isotropic dimensionless permeability.

2.6.2. Orthotropy. Following the general framework proposed in [32], we can establish the flow law of a power-law fluids through an orthotropic porous medium with privileged directions  $\mathbf{e}_1, \mathbf{e}_2, \mathbf{e}_3$  as

$$\begin{aligned} \nabla p^{(0)} = & - \frac{\mu_0}{l^2} \times \left( \frac{1}{k_1^*} \left( \frac{|\langle v_1^{(0)} \rangle|}{l} \right)^{n-1} \langle v_1^{(0)} \rangle \mathbf{e}_1 + \frac{1}{k_2^*} \left( \frac{|\langle v_2^{(0)} \rangle|}{l} \right)^{n-1} \langle v_2^{(0)} \rangle \mathbf{e}_2 \right. \\ & \left. + \frac{1}{k_3^*} \left( \frac{|\langle v_3^{(0)} \rangle|}{l} \right)^{n-1} \langle v_3^{(0)} \rangle \mathbf{e}_3 \right), \end{aligned} \tag{35}$$

where  $k_1^*$ ,  $k_2^*$  and  $k_3^*$  are three rheological functions that may depend on  $n$  and the geometry of the porous medium. When  $n \neq 1$ ,  $k_1^*$  also depends on  $|\langle v_2^{(0)} \rangle / \langle v_1^{(0)} \rangle|$ ;  $k_2^*$  on  $|\langle v_3^{(0)} \rangle / \langle v_1^{(0)} \rangle|$  and  $|\langle v_1^{(0)} \rangle / \langle v_2^{(0)} \rangle|$ ; and  $k_3^*$  on  $|\langle v_3^{(0)} \rangle / \langle v_2^{(0)} \rangle|$ ,  $|\langle v_1^{(0)} \rangle / \langle v_3^{(0)} \rangle|$  and  $|\langle v_2^{(0)} \rangle / \langle v_3^{(0)} \rangle|$ ; respectively. When  $n = 1$ , the flow law is linear so that  $k_1^*$ ,  $k_2^*$  and  $k_3^*$  stands for the usual principal components of the dimensionless orthotropic tensor.

### 3. Numerical investigations of the macroscopic flow law

The upscaling technique described earlier is of great interest since it gives us the general form and properties of the macroscopic flow law. The objective of this section is to highlight, more precisely, the influence of the microstructure of the porous media on the flow law. For this purpose, we consider the flow perpendicular to the square and triangular arrays of infinite and parallel fibres of circular cross-section. Therefore, numerical simulations have been performed with simple two-dimensional periodic arrays of circular inclusions. After a brief description of these two-dimensional microstructures under consideration (section 3.1), the numerical method used is given in section 3.2. The general form of their associated flow law is presented in section 3.3, and the numerical results are given in sections 3.5 and 3.4.

#### 3.1. Description of the two-dimensional microstructures

The porous media under consideration are circular solid inclusions of identical radius  $a$ , arranged in periodic patterns such as square and triangular arrays.

*3.1.1. Square arrays of circular inclusions (figure 2).* The size of the periodic REV is  $l$ . The solid fraction of the porous media,  $c = (\pi a^2)/l^2$ , varies from 0 to  $c_{\max} = \pi/4$ . These two-dimensional microstructures display four material symmetry axis (dashed-dotted lines in figure 2):  $e_1$ ,  $e_2$ , the other two being observed at  $e_1 + e_2$  and  $e_2 - e_1$ . In that sense, these microstructures exhibit tetratrophy: they are invariant through any rotation of angle  $\kappa\pi/2$ , where  $\kappa$  is an integer.

*3.1.2. Triangular arrays of circular inclusions (figure 3).* In this case, the sizes of the periodic cell are  $l$  and  $\sqrt{3}l$ . Thus, the solid fraction of the porous media,  $c = (2\pi a^2)/(\sqrt{3}l^2)$ , varies from 0 to  $c_{\max} = \pi/(2\sqrt{3})$ . These microstructures exhibit hexatrophy, since they have six material symmetry axis (dashed-dotted lines in figure 3):  $e_1$ ,  $e_2$ , the other four being located at  $\pi/6$ ,  $\pi/3$ ,  $2\pi/3$  and  $5\pi/6$  from the  $e_1$  axis. In other words, the triangular microstructures are invariant through any rotation of angle  $\kappa\pi/3$ .

#### 3.2. Numerical method

Numerical results presented in the following have been obtained:

(a) Solving the boundary problem (18)–(20) in dimensional form on the periodic REV  $\Omega$ ,

$$2\mu_0 \nabla \cdot ((\dot{\gamma}_{\text{eq}}^{(0)})^{n-1} D^{(0)}) = \nabla p^{(1)} + \nabla p^{(0)} \quad \text{in } \Omega_1, \quad (36)$$

$$\nabla \cdot \mathbf{v}^{(0)} = 0 \quad \text{in } \Omega_1, \quad (37)$$

$$\mathbf{v}^{(0)} = 0 \quad \text{on } \Gamma, \quad (38)$$

where the unknowns  $\mathbf{v}^{(0)}$  and  $p^{(1)}$  are periodic, and where the macroscopic pressure drop  $\nabla p^{(0)}$  is a given source term. More precisely, as illustrated in figures 2 and 3, both

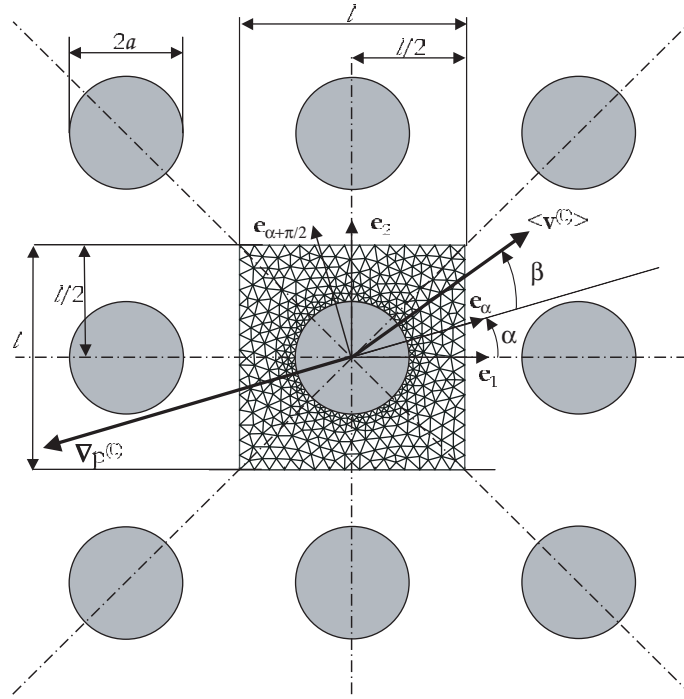


**Figure 2.** Square array of circular solid inclusions. The periodic REV of such a microstructure is given by the centred finite element mesh (used to run the simulation).

microstructures were submitted to a macroscopic pressure gradient  $\nabla p^{(0)}$  of intensity  $\|\nabla p^{(0)}\|$ ,

$$\nabla p^{(0)} = -\|\nabla p^{(0)}\|e_\alpha = -\|\nabla p^{(0)}\|(\cos(\alpha)e_1 + \sin(\alpha)e_2), \quad (39)$$

where  $\alpha = (\widehat{e_1, e_\alpha})$ . The boundary-value problem (36)–(38) was solved with a mixed pressure–velocity finite element formulation implemented in the software Femlab® [36]. A quadratic P2 and a linear P1 polynomial approximation were adopted for the velocity field  $v^{(0)}$  and the pressure  $p^{(1)}$ , respectively.

- (b) Calculating the magnitude of the cell-averaged fluid velocity  $\langle v^{(0)} \rangle$  to obtain the macroscopic flow law. The resulting macroscopic velocity field  $\langle v^{(0)} \rangle$  of intensity  $\|\langle v^{(0)} \rangle\|$  generally exhibited an angle  $\beta$  from the vector  $e_\alpha$  (see figures 2 and 3),

$$\langle v^{(0)} \rangle = \|\langle v^{(0)} \rangle\|(\cos(\alpha + \beta)e_1 + \sin(\alpha + \beta)e_2) = ue_1 + ve_2 \quad (40)$$

or

$$\langle v^{(0)} \rangle = \|\langle v^{(0)} \rangle\|(\cos(\beta)e_\alpha + \sin(\beta)e_{\alpha+(\pi/2)}) = u'e_\alpha + v'e_{\alpha+(\pi/2)}. \quad (41)$$

The above procedure has been carried out on both microstructures, for power-law exponent  $n$  and solid fraction  $c$  ranging from 0.3 to 1.5, and from 0.01 to  $(c_{\max} - 0.01)$ , respectively.

### 3.3. General form of the macroscopic flow law for both microstructures

In most works concerning the modelling of the flow through porous media similar to those depicted in figures 2 and 3, i.e. involving circular solid inclusions of constant radius  $a$ , the

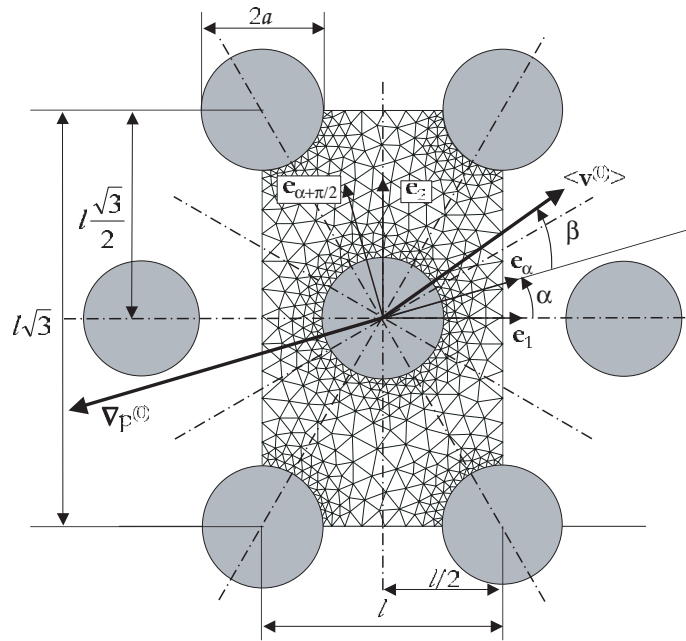


**Figure 3.** Triangular array of circular solid inclusions. The periodic REV of such a microstructure is given by the centred finite element mesh (used to run the simulation).

microscopic characteristic length  $l$  is arbitrarily linked to the inclusion radius. In order to compare our results with those obtained in these works, we also suppose that  $l = a$ . Note that the two types of microstructures have two identical orthogonal symmetry axis, i.e.  $e_1$  and  $e_2$ . It is therefore possible to express the flow through such microstructures using an orthotropic flow law such as (35). In the  $(e_1, e_2)$  plane, this leads to

$$\nabla p^{(0)} = -\frac{\mu_0}{a^2} \left( \frac{1}{k_1^*} \left( \frac{|u|}{a} \right)^{n-1} u e_1 + \frac{1}{k_2^*} \left( \frac{|v|}{a} \right)^{n-1} v e_2 \right), \quad (42)$$

where the  $k_i^*$  depend on the solid fraction  $c$ , the exponent  $n$  and the ratio  $|u/v|$ , i.e. the angle  $\alpha + \beta$ :  $k_i^* = k_i^*(c, n, \alpha + \beta)$ .

### 3.4. Numerical results: on-axis flow

A first set of 'numerical experiments' was performed with  $\alpha = \kappa\pi/\lambda$ , i.e. along the symmetry axis of the microstructures ( $\lambda$ , respectively, equals 4 or 6 for the square or triangular arrays, and  $\kappa$  being a given integer). In all these calculations, the macroscopic velocity  $\langle v^{(0)} \rangle$  was such that

$$\forall \kappa \in \mathbb{N}, \quad \beta \left( \alpha = \kappa \frac{\pi}{\lambda} \right) = 0. \quad (43)$$

This result, which could have been proved without the simulation (see appendix), is a direct consequence of the symmetry property: the macroscopic velocity must be aligned with the imposed pressure gradient when the latter is in the direction of one of the symmetry axes. Moreover, due to the invariance of the microstructures through any rotation of angle  $2\kappa\pi/\lambda$ ,

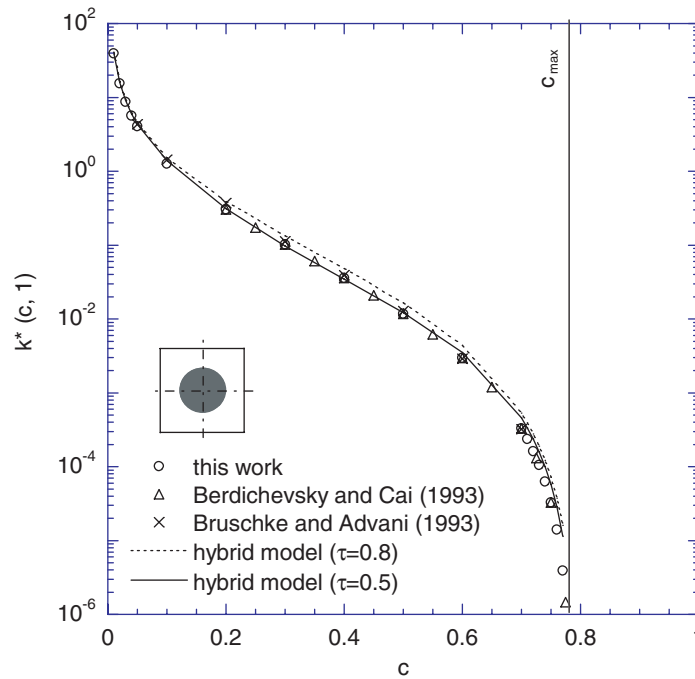


**Figure 4.** Square array of cylinders. Evolution of the dimensionless permeability  $k^*(c, 1)$  with the solid fraction  $c$ . Marks represent simulation results, lines show the prediction of analytical models.

it was systematically found that

$$\forall \kappa \in \mathbb{N}, \quad u' \left( \alpha = 2\kappa \frac{\pi}{\lambda} \right) = u'(\alpha = 0), \quad u' \left( (2\kappa + 1) \frac{\pi}{\lambda} \right) = u' \left( \frac{\pi}{\lambda} \right). \quad (44)$$

The flow along the  $e_1$  axis ( $\alpha = 0$ ) was then more precisely studied. In this situation, one can write, in accordance with (42),

$$\frac{\partial p^{(0)}}{\partial X_1} = - \frac{\mu_0}{a^2 k^*(c, n)} \left[ \frac{u}{a} \right]^{n-1} u, \quad (45)$$

where  $k^*(c, n) = k_1^*(c, n, \alpha + \beta = 0)$ .

Figures 4 and 5 show the evolution of  $k^*(c, 1)$  with the solid fraction  $c$  for the square and triangular array of cylinders, respectively. For both microstructures,  $k^*$  is a decreasing function of  $c$ , and tends towards infinite when  $c \rightarrow 0$  and 0 when  $c \rightarrow c_{\max}$ . To validate our methodology, simulation results were compared with analytical and numerical models cited in the literature:

- (a) For the two investigated microstructures, figures 4 and 5 prove that the current results are in very good accordance with numerical results obtained by previous authors [3, 25].
- (b) For the square microstructure, Bruschke and Advani [25] proposed a semi-analytical hybrid expression of  $k^* = k_{\text{hyb}}^*$ , which is a phenomenological combination of the analytical cell model  $k_{\text{cell}}^*$  [9, 14], known to give good prediction within the low solid fraction range, and the analytical lubrication model  $k_{\text{lub}}^*$  [37], which is much more accurate at high solid fractions:

$$k_{\text{hyb}}^*(c, 1) = \xi_1 k_{\text{lub}}^*(c, 1) + \xi_2 k_{\text{cell}}^*(c, 1) \quad (46)$$

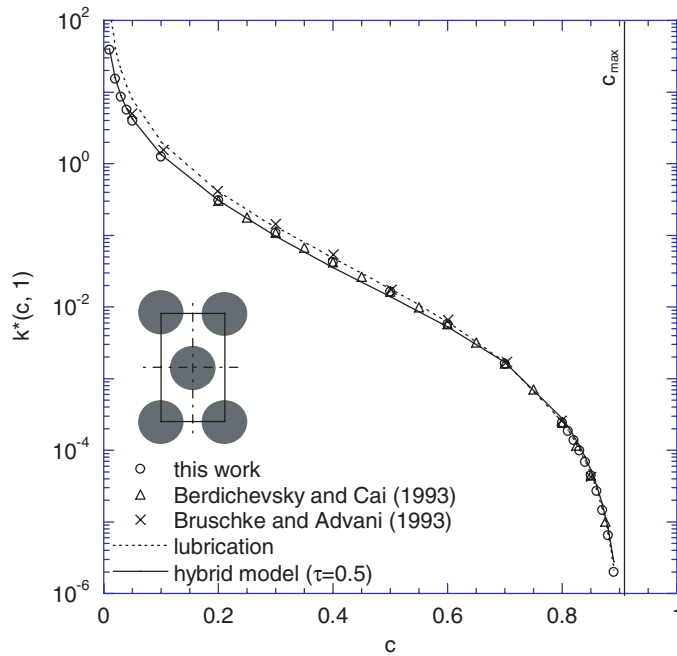


**Figure 5.** Triangular array of cylinders. Evolution of the dimensionless permeability  $k^*(c, 1)$  with the solid fraction  $c$ . Marks represent simulation results, lines show the prediction of analytical models.

with,

$$\xi_1 = 1 - e^{\tau(\Phi/(\Phi-1))}, \quad \xi_2 = 1 - e^{\tau((\Phi-1)/\Phi)}, \quad (47)$$

$$k_{cell}^*(c, 1) = -\frac{1}{8c} \left( \ln c + \frac{3}{2} - 2c + \frac{1}{2}c^2 \right), \quad (48)$$

$$k_{lub}^*(c, 1) = \frac{1}{3A} \frac{(1 - \Phi)^2}{\sqrt{\Phi}^3} \left( 3\sqrt{\Phi} \frac{\arctan(\sqrt{(1 + \sqrt{\Phi})/(1 - \sqrt{\Phi})})}{\sqrt{1 - \Phi}} + \frac{1}{2}\Phi + 1 \right)^{-1}, \quad (49)$$

where  $\Phi = c/c_{max}$ ,  $A = 1$  and  $A = \sqrt{3}$  for the square array and the triangular array of cylinders, respectively. The parameter  $\tau$  is adjusted on the numerical data. Brusckhe and Advani [25] proposed to choose  $\tau = 0.8$ . In the case of a triangular array of cylinders, the lubrication model was sufficient to fit their numerical results [25]. As shown in figures 4 and 5, a better fit of our numerical results (and also Berdichevsky and Cai’s [3] numerical data) is obtained with the hybrid approximation, by using  $\tau = 0.5$  for both microstructures.

The dimensionless permeability  $k^*(c, n)$  when  $n \neq 1$  was also estimated from our numerical simulations. The evolution of this parameter with the solid fraction  $c$  and for several values of  $n$  is illustrated in figures 6 and 7 for the square and triangular arrays, respectively. For both microstructures, it is found that  $k^*(c, n)$  is still a decreasing function of  $c$ , the trends underlined in the Newtonian case still being valid. Likewise, as shown in figure 6, note that a fairly good correlation is recorded between numerical results obtained by Brusckhe and

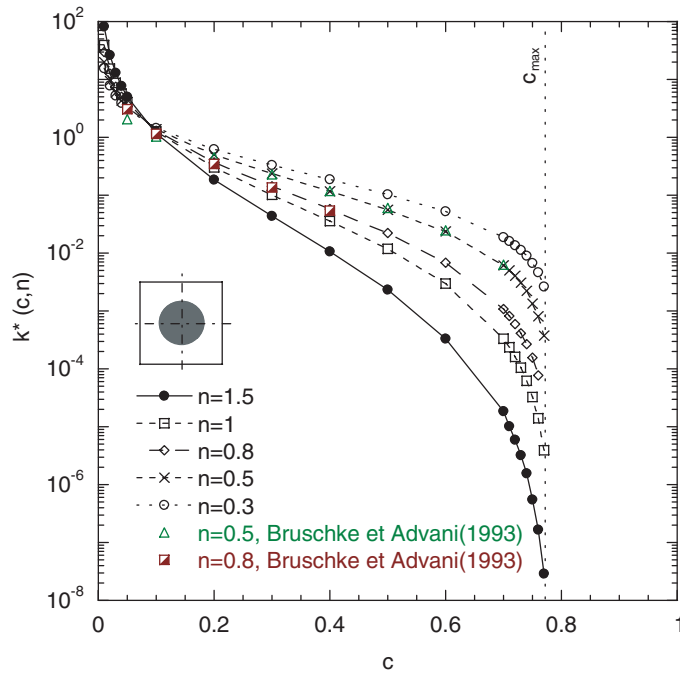


**Figure 6.** Square array of cylinders. Evolution of the dimensionless permeability  $k^*(c, n)$  with the solid fraction  $c$  for various power-law exponent  $n$ .

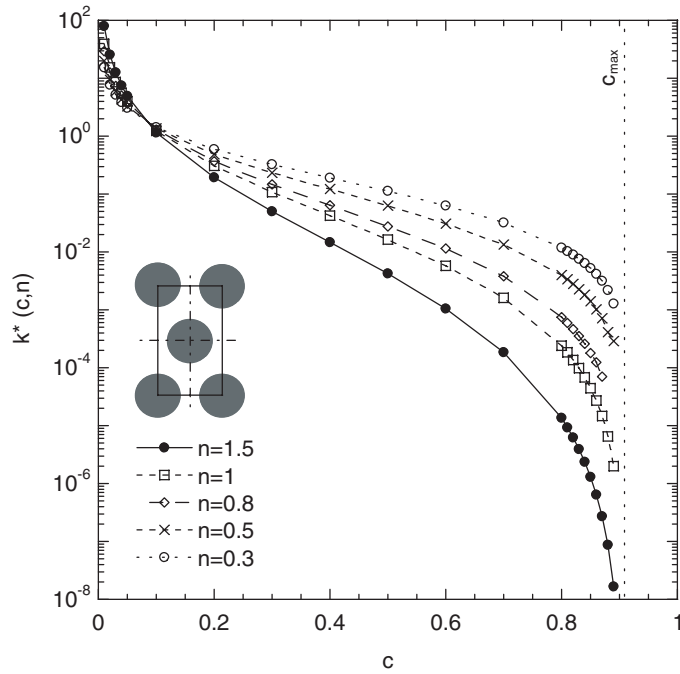


**Figure 7.** Triangular array of cylinders. Evolution of the dimensionless permeability  $k^*(c, n)$  with the solid fraction  $c$  for various power-law exponent  $n$ .

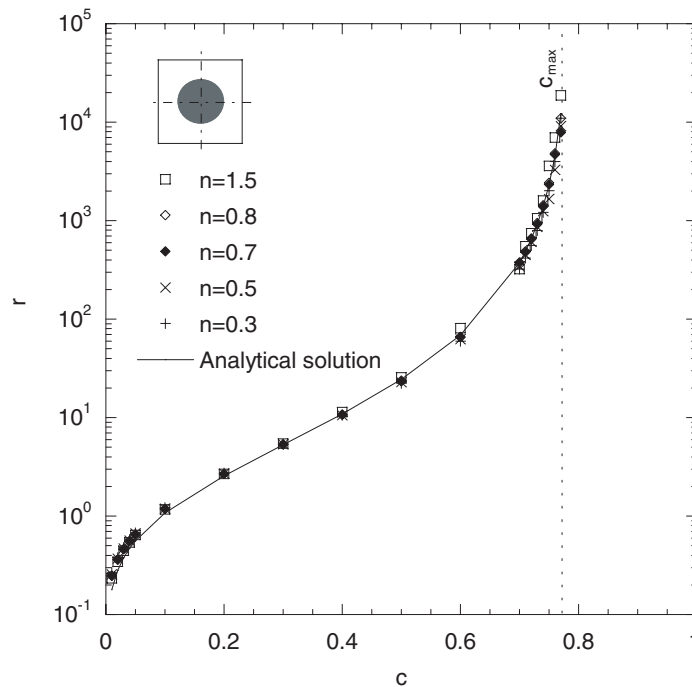


**Figure 8.** Square array of cylinders. Evolution of the dimensionless function  $r$  with the solid fraction  $c$  and for various power-law exponents  $n$ . The continuous line is the prediction given by (50) with  $\psi = 0.80$ .

Advani [25] and ours. Adopting a reasoning similar to that initially proposed in [25], we have estimated the evolution of the dimensionless functions  $r = [k^*(c, n)/k^*(c, 1)]^{1/(1-n)}$  for the two types of microstructures and for  $n \neq 1$ . Figures 8 and 9 show that it is reasonable to consider that inside the tested solid fraction range,  $r$  is  $n$ -independent and depends only on the microstructure and the solid fraction  $c$ . Based on numerical results obtained in this work and those gained in [28], a suitable expression for  $r$  is proposed

$$r = \frac{\sqrt{\Phi}}{\psi(1 - \sqrt{\Phi})^2}, \quad (50)$$

where  $\psi$  is a constant. Figures 8 and 9 show that our numerical data can be fitted by the above relation using  $\psi = 0.80$  and  $0.65$  for the square and triangular array of cylinders, respectively. As a consequence, the on-axis dimensionless permeability  $k^*(c, n)$  can be deduced directly from  $k^*(c, 1)$  using (50).

### 3.5. Numerical results: off-axis flow

We now focus on situations for which  $\alpha$  can be different from  $\kappa\pi/\lambda$ , to study the anisotropy of the flow law more precisely. For this purpose, several ‘numerical experiments’ were performed on the REV’s using macroscopic pressure gradients  $\nabla p^{(0)}(\alpha)$  of same intensity  $\|\nabla p^{(0)}\|$  and for which  $0 \leq \alpha \leq \pi$ . It was hence possible to determine the angle  $\beta(\alpha)$  and the components  $u'(\alpha)$  and  $v'(\alpha)$  of the resulting macroscopic velocity fields  $\langle v^{(0)} \rangle(\alpha)$ . As examples, figures 10 and 11 show for the two types of arrangement the evolutions of the angle  $\beta$  and of the normalized components  $u'(\alpha)/u'(0)$  and  $v'(\alpha)/v'(0)$  as functions of  $\alpha$ , for various solid fractions and

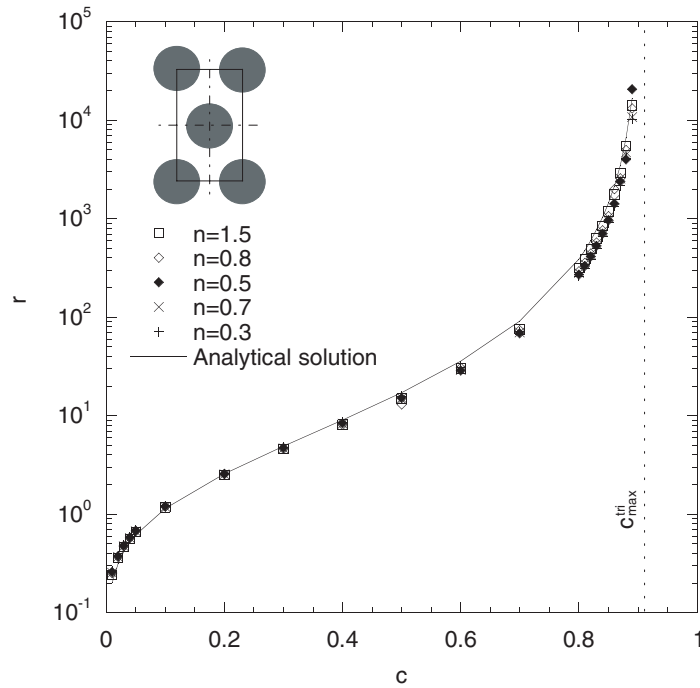


**Figure 9.** Triangular array of cylinders. Evolution of the dimensionless function  $r$  with the solid fraction  $c$  and for various power-law exponents  $n$ . The continuous line is the prediction given by (50) with  $\psi = 0.65$ .

power-law exponents. Several comments can be formulated from these figures. They are listed in the following.

- (a) For  $n \neq 1$ , figures 10 and 11 clearly reveal (i) that the macroscopic velocity field is not aligned with the macroscopic pressure gradient, except when  $\alpha = \kappa\pi/\lambda$  and (ii) that the macroscopic flow law exhibits tetratropy in the case of square microstructures and hexatropy for triangular ones:

$$\forall \alpha \in \mathbb{R}, \quad \kappa \in \mathbb{N}, \quad \begin{cases} \beta\left(\alpha + 2\kappa\frac{\pi}{\lambda}\right) = \beta(\alpha), \\ u'\left(\alpha + 2\kappa\frac{\pi}{\lambda}\right) = u'(\alpha), \\ v'\left(\alpha + 2\kappa\frac{\pi}{\lambda}\right) = v'(\alpha). \end{cases} \quad (51)$$

Once again, this is directly connected to the invariance of the studied microstructures through any rotation of angle  $2\kappa\pi/\lambda$ .

- (b) For  $n = 1$ , numerical results show (i) that  $\langle v^{(0)} \rangle$  is always aligned with  $p^{(0)}$  and (ii) that the macroscopic flow is isotropic, even if the microstructures studied exhibit tetratropy (square) or hexatropy (triangular):

$$\forall \alpha \in \mathbb{R}, \quad \kappa \in \mathbb{N}, \quad \begin{cases} \beta(\alpha) = \beta(0) = 0, \\ u'(\alpha) = u'(0), \\ v'(\alpha) = v'(0). \end{cases} \quad (52)$$

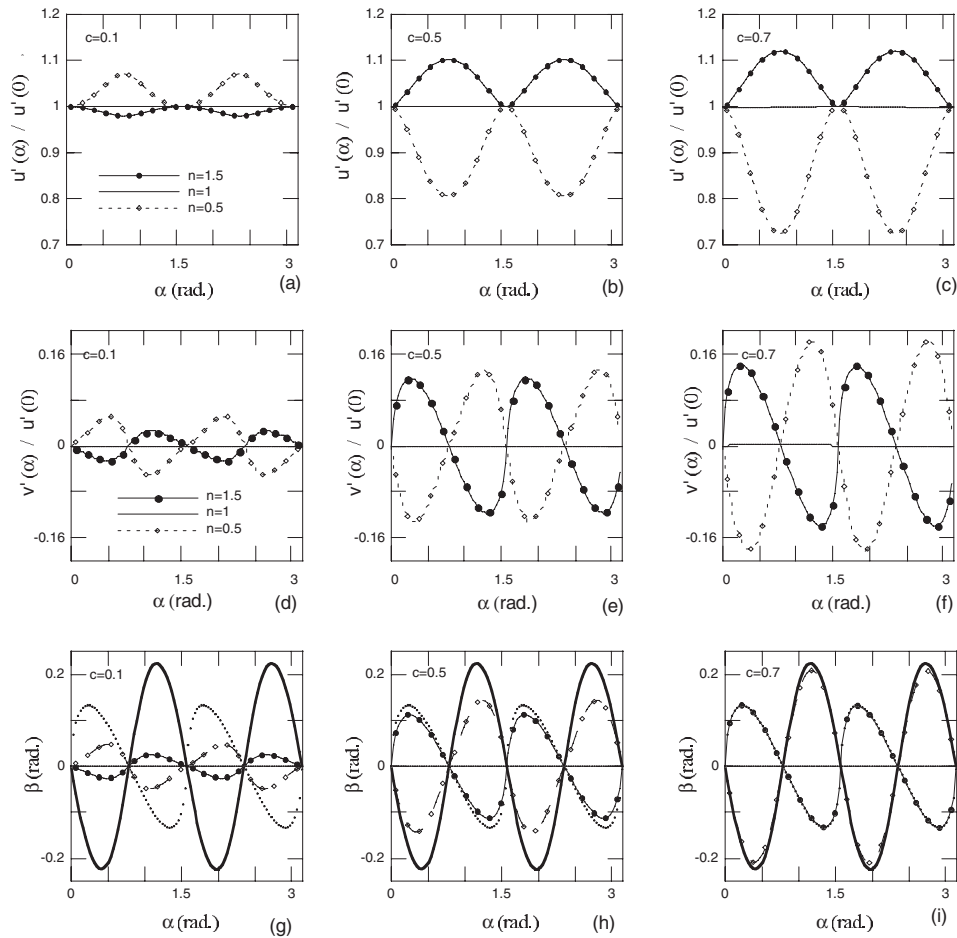


**Figure 10.** Square array of cylinders. Evolutions of the normalized components  $u'(\alpha)/u'(0)$  (a)–(c),  $v'(\alpha)/u'(0)$ ; (d)–(f) and of the angle  $\beta$ ; (g)–(i) as functions of  $\alpha$ , for various solid fractions and power-law exponents. The bold dashed ( $n = 1.5$ ) and continuous lines ( $n = 0.5$ ) are the prediction given by (54).

The last result can be proved theoretically considering both the invariance through any rotation of angle  $2\kappa\pi/\lambda$  and the weak formulation (23) deduced from the homogenization process, that shows that  $\langle v^{(0)} \rangle$  is a linear function of  $\nabla p^{(0)}$  (see appendix).

- (c) The signs of the deviations  $\Delta\beta(\alpha) = \beta(\alpha) - \beta(0)$ ,  $\Delta u'(\alpha) = u'(\alpha) - u'(0)$  and  $\Delta v'(\alpha) = v'(\alpha) - v'(0)$  always differ as the fluid is shear thinning ( $n < 1$ ) or shear thickening ( $n > 1$ ).
- (d) Comparing, respectively, figures 10(a), (d) and (g) with figures 10(b), (e) and (h) one can see that the signs of  $\Delta\beta$ ,  $\Delta u'$  and  $\Delta v'$  when  $n \neq 1$  can also change with the solid fraction.
- (e) At a given solid fraction and power-law exponent  $n$ , the anisotropy of the square arrangements is more pronounced than that of the triangular ones. The maximal deviations  $|\Delta\beta|_{\max}$ ,  $|\Delta u'|_{\max}$  and  $|\Delta v'|_{\max}$  are systematically larger in the case of the square microstructures.
- (f) The lower the solid fraction, the less pronounced the anisotropy;  $|\Delta\beta|_{\max}$ ,  $|\Delta u'|_{\max}$  and  $|\Delta v'|_{\max}$  tend to 0 as  $c \rightarrow 0$ .

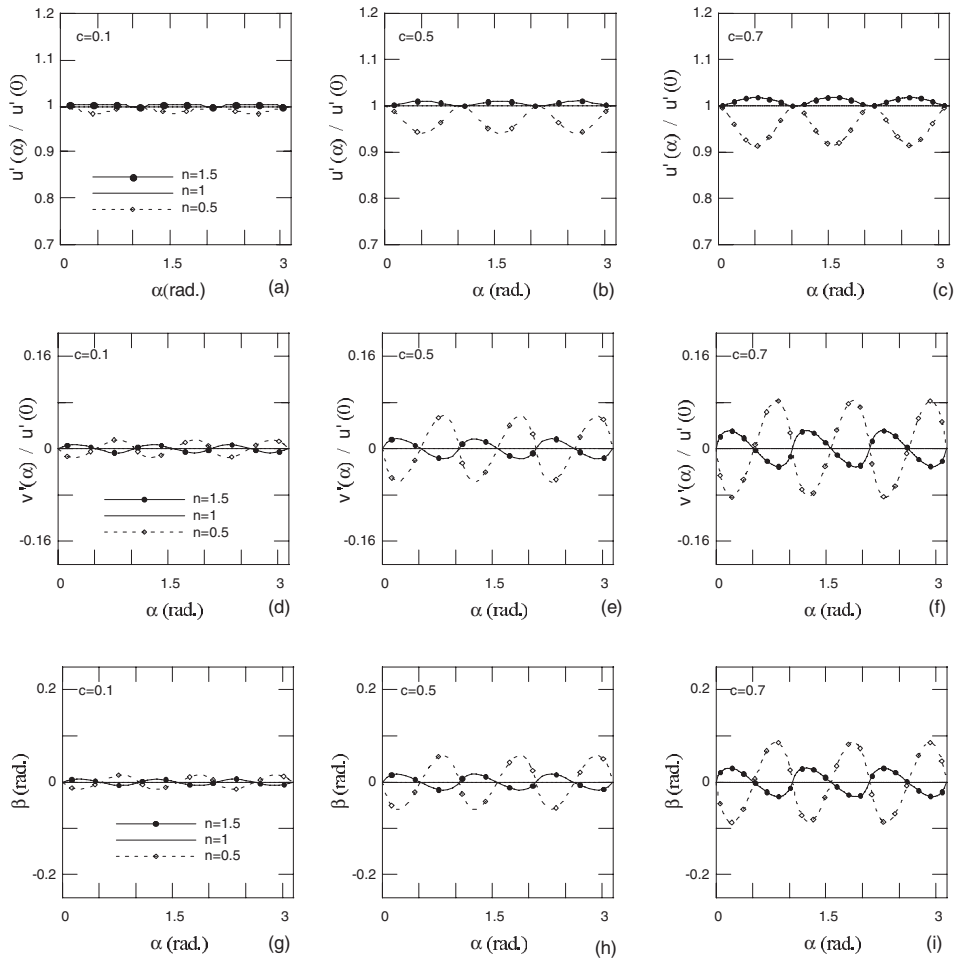


**Figure 11.** Triangular array of cylinders. Evolutions of the normalized components  $u'(\alpha)/u'(0)$  (a)–(c),  $v'(\alpha)/u'(0)$  (d)–(f) and of the angle  $\beta$  (g)–(i) as functions of  $\alpha$ , for various solid fractions and power-law exponents.

### 3.6. Discussion

Numerical results obtained in the two previous subsections have underlined the strong and coupled influence on the macroscopic flow response of the fluid rheology and of the geometry of the microstructures. If analytical macroscopic expressions can account for such complex flow in the case of on-axis situations (see section 3.4, [25]), little has been done in the case of off-axis situations. For instance, it is of interest to see if off-axis macroscopic flows can be easily deduced from on-axis flows in the  $e_1$  and  $e_2$  directions. Based on simulation results of the flow of power-law fluid through square arrays of circular [28] and elliptic [29] inclusions, Woods *et al* [29] have recently tried to do so. For this purpose, the authors proposed a simple form of the macroscopic flow law expressed in the  $(e_1, e_2)$  reference frame. In the case of circular inclusions, this law becomes

$$\nabla p^{(0)} = -\frac{\mu_0}{k^* a^2} \left( \left( \frac{|u|}{a} \right)^{n-1} u e_1 + \left( \frac{|v|}{a} \right)^{n-1} v e_2 \right). \quad (53)$$

Note that this relation is a particular case of equation (42) with  $k_1^*(c, n, \alpha + \beta)^* = k_2^*(c, n, \alpha + \beta) = k^*(c, n)$ . This macroscopic model brings up the following comments:

- At the macroscopic scale, equation (53) suggests that a macroscopic velocity field  $\langle v^{(0)} \rangle = ue_1 + ve_2$  resulting from an imposed pressure gradient  $\nabla p^{(0)} = \cos(\alpha)e_1 + \sin(\alpha)e_2$  is the summation of  $\langle v_1^{(0)} \rangle = ue_1$  and  $\langle v_2^{(0)} \rangle = ve_2$ , respectively, resulting from on-axis imposed pressure gradients  $\cos(\alpha)e_1$  and  $\sin(\alpha)e_2$ . Furthermore, from (40), (41) and (53), it can be easily shown that the angle  $\beta$  between the macroscopic velocity field and the macroscopic imposed pressure gradient is in the form,

$$\beta = \arctan \left[ [\tan \alpha]^{1/n} \right] - \alpha. \quad (54)$$

According to (54), angle  $\beta$  does not depend on the solid fraction  $c$ . As shown in figure 10, if (54) fairly well reproduces numerical experiments at solid fractions close to  $c_{\max}$ , the lower the solid fraction, the larger is the deviation of (54) from the simulation.

- At the microscopic scale, equation (53) also suggests that the local velocity field  $v^{(0)}$  resulting from an imposed pressure gradient  $\nabla p^{(0)} = \cos(\alpha)e_1 + \sin(\alpha)e_2$  is also the summation of  $v_1^{(0)}$  and  $v_2^{(0)}$  resulting from on-axis imposed pressure gradients  $\cos(\alpha)e_1$  and  $\sin(\alpha)e_2$ , respectively. In order to check the validity of such an assumption, different numerical simulations were achieved with a shear thinning fluid ( $n = 0.5$ ) and with two square microstructures with a solid volume fraction  $c = 0.1$  (i.e. rather low) and  $0.7$  (i.e. close to  $c_{\max}$ ), respectively. Figures 12(a)–(d) show the local velocity field  $v^{(0)}$  (arrows) and its corresponding local shear stress  $\tau = \mu_0(\gamma_{\text{eq}}^{(0)})^n$  (colour map) computed by following two different ways. Figures 12(a) and (c) show the above fields computed with an imposed gradient of pressure  $\nabla p^{(0)} = \cos(\pi/8)e_1 + \sin(\pi/8)e_2$ . Figures 12(b) and (d) show now the same fields obtained by summing the results of two different simulations performed with imposed gradients of pressure  $\nabla p^{(0)} = \cos(\pi/8)e_1$  and  $\nabla p^{(0)} = \sin(\pi/8)e_2$ , respectively. In this later case, we have  $v^{(0)} = v_1^{(0)} + v_2^{(0)}$ . At high solid fraction, figures 12(a) and (b) show a fairly good correlation between the numerical experiments obtained by the two different ways: the local velocities and the shear stress patterns are almost identical. This reinforces the validation of (53) for square arrays of circular inclusions at high solid fraction. Such a good comparison is mainly due to the fact that the main sheared zones are concentrated in the small gaps between the inclusions and do not interact together. At low solid fraction, this reasoning breaks down, as it becomes evident by comparing figures 12(c) and (d); a significant difference is observed on the local velocity field as well as on the local shear stress state. This points out that the form of (53) is not valuable to describe flows at mild or low solid fractions. Similar conclusions have been obtained with a shear thickening fluid ( $n > 1$ ).

#### 4. Conclusion

In this work, a rigorous upscaling technique was used to derive the general structure and properties of the flow law of a power-law fluid through an anisotropic fibrous medium. In particular, it was proved without prerequisites at the macroscopic scale that the macroscopic pressure gradient was an anisotropic homogeneous function of degree  $n$  of the macroscopic velocity field,  $n$  being the power law exponent of the flowing fluid.

It is possible to explore quantitatively the as-derived flow law by solving numerically the REV boundary-value problems directly deduced from the upscaling process. In this paper, such a methodology was illustrated and applied on two very simple types of two-dimensional anisotropic porous media, i.e. square or triangular arrays of circular solid inclusions.

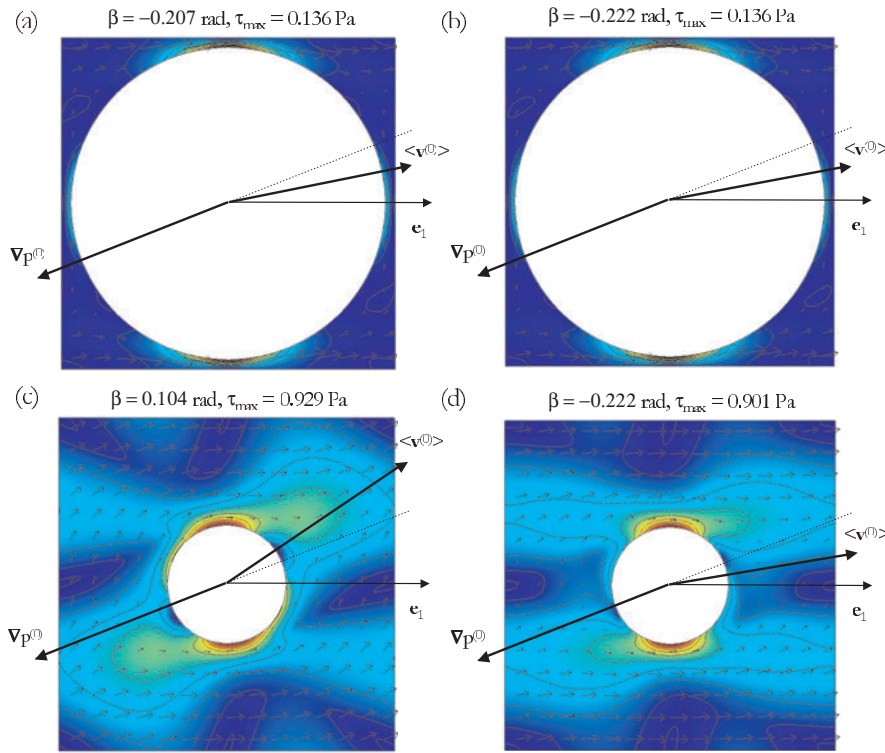


**Figure 12.** Flow of a shear thinning fluid ( $\mu_0 = 1 \text{ Pa s}$ ,  $n = 0.5$ ) through a square array of circular solid inclusions ( $l = 1 \text{ m}$ ,  $c = 0.7$  (a) and (b) and  $c = 0.1$  (c) and (d)). Representation of the local velocity field  $\mathbf{v}^{(0)}$  (arrows) and its corresponding local shear stress  $\tau = \mu_0(\gamma_{\text{eq}}^{(0)})^n$  (colour map) computed by following two different ways: results in (a) and (c) were computed with an imposed gradient of pressure  $\nabla p^{(0)} = \cos(\pi/8)\mathbf{e}_1 + \sin(\pi/8)\mathbf{e}_2$ . Results in (b) and (d) are the sum of the results of two different simulations performed with imposed gradients of pressure  $\nabla p^{(0)} = \cos(\pi/8)\mathbf{e}_1$  and  $\nabla p^{(0)} = \sin(\pi/8)\mathbf{e}_2$ , respectively. The linear colour scale used for the shear stress  $\tau$  ranges from 0 (blue) to  $\tau_{\text{max}}$  (red).

When it was possible, numerical results were successfully compared with those reported in the literature, thus, validating the present methodology. Results have also underlined the significant role of the solid fraction, the fluid rheology and the porous media anisotropy on the resulting macroscopic flow law. Likewise, if simulated on-axis flows were successfully fitted with analytical or phenomenological continuous expressions proposed in the literature, it has been shown that further effort would be required to perform similar fits with simulated off-axis flows.

Future planned works will: (i) propose some guidelines to establish and fit a suitable tensorial form of macroscopic flow law for a given fibrous medium and (ii) apply the whole methodology to more complex fibrous media.

## Appendix

As an example, we now consider a square array of cylinder with circular cross-section. The cylinder axes are in the direction  $\mathbf{e}_3$ . The porous medium can be considered as an orthotropic medium with privileged directions  $\mathbf{e}_1, \mathbf{e}_2, \mathbf{e}_3$ , with a flow law that is invariant

through any rotation of angle  $\pi/2$  around  $e_3$ . Assuming that the flow is perpendicular to the square array of cylinders,  $\nabla p^{(0)} = (\nabla_1 p^{(0)}, \nabla_2 p^{(0)}, 0)$ , the flow law (35) reduces to

$$\nabla p^{(0)} = -\frac{\mu_0}{l^2} \left( \frac{1}{k_1^*} \left( \frac{|\langle v_1^{(0)} \rangle|}{l} \right)^{n-1} \langle v_1^{(0)} \rangle e_1 + \frac{1}{k_2^*} \left( \frac{|\langle v_2^{(0)} \rangle|}{l} \right)^{n-1} \langle v_2^{(0)} \rangle e_2 \right), \quad (\text{A1})$$

where,

$$k_1^* = k_1^* \left( c, n, \left| \frac{\langle v_2^{(0)} \rangle}{\langle v_1^{(0)} \rangle} \right| \right), \quad (\text{A2})$$

$$k_2^* = k_2^* \left( c, n, \left| \frac{\langle v_1^{(0)} \rangle}{\langle v_2^{(0)} \rangle} \right| \right). \quad (\text{A3})$$

The velocity  $\langle v^{(0)} \rangle = (\langle v_1^{(0)} \rangle, \langle v_2^{(0)} \rangle, 0)$  causes the gradient of pressure  $\nabla p^{(0)} = (\nabla_1 p^{(0)}, \nabla_2 p^{(0)}, 0)$ . Due to the symmetry shown by the array of circular cylinders, the flow law is invariant through any rotation of angle  $\pi/2$  around  $e_3$ . Therefore, a velocity  $\langle v^{(0)} \rangle = (-\langle v_2^{(0)} \rangle, \langle v_1^{(0)} \rangle, 0)$  causes a macroscopic gradient  $\nabla p^{(0)} = (-\nabla_2 p^{(0)}, \nabla_1 p^{(0)}, 0)$ . Thus, from (A1) we get,

$$k_1^* \left( c, n, \left| \frac{\langle v_2^{(0)} \rangle}{\langle v_1^{(0)} \rangle} \right| \right) = k_2^* \left( c, n, \left| \frac{\langle v_2^{(0)} \rangle}{\langle v_1^{(0)} \rangle} \right| \right) \quad (\text{A4})$$

or

$$k_1^*(c, n, X) = k_2^* \left( c, n, \frac{1}{X} \right) \quad \text{with } X = \left| \frac{\langle v_2^{(0)} \rangle}{\langle v_1^{(0)} \rangle} \right|. \quad (\text{A5})$$

This last relation characterizes the most general form of the flow law across the array of cylinder. The macroscopic velocity is colinear to the gradient of pressure when this gradient of pressure is parallel to the four axes of symmetry  $e_1$ ,  $e_2$ ,  $e_1 + e_2$  and  $e_1 - e_2$ . For other directions, the velocity is no more colinear to the gradient of pressure. Velocity  $\|\langle v^{(0)} \rangle\|$  is a periodic function of  $\alpha = (e_1, \nabla p^{(0)})$ , of period  $\pi/2$ . This periodicity characterizes the two-dimensional tetratrophy of the flow law through the isotropic porous medium in consideration. Finally, in the case where  $n = 1$ , the relation (A1) becomes isotropic ( $k_1^* = k_2^* = k^*(c)$ ),

$$\nabla p^{(0)} = -\frac{\mu_0}{k^* l^2} (\langle v_1^{(0)} \rangle e_1 + \langle v_2^{(0)} \rangle e_2). \quad (\text{A6})$$

Following the same reasoning, similar results can be obtained for the triangular microstructure: the macroscopic velocity is colinear to the gradient of pressure only when this gradient of pressure is parallel to the six axes of symmetry, when  $n \neq 1$  the flow law exhibits hexatrophy and when  $n = 1$ , the flow law is isotropic.

## References

- [1] Darcy H 1856 *Les Fontaines Publiques de la Ville de Dijon* (Paris: Victor Valmont)
- [2] Advani S G, Bruschke M V and Parnas R S 1994 Flow and rheology in polymer composites manufacturing *Resin Transfer Molding flow Phenomena in Polymeric Composites* (Amsterdam: Elsevier) chapter 12, pp 465–515
- [3] Berdichevsky A L and Cai Z 1993 Perform permeability predictions by self consistent method and finite element simulation *Polym. Composites* **14** 132–143
- [4] Boutin C 2000 Study of permeability by periodic and self consistent homogenisation. *Eur. J. Mech. A/Solids* **19** 603–32
- [5] Clague D S and Philips R J 1997 A numerical calculation of the hydraulic permeability of three dimensional disordered fibrous media *Phys. Fluids* **9** 1562–72

- [6] Drummond J E and Tahir M I 1984 Laminar viscous flow through regular arrays of parallel solid cylinders *Int. J. Multiphase Flow* **10** 515–40
- [7] Edwards D A, Shapiro M, Bar Yoseph P and Shapira M 1990 The influence of reynolds number upon the apparent permeability of spatially periodic arrays of cylinders *Phys. Fluids A*. **2** 45–55
- [8] Ghaddar C K 1995 On the permeability of unidirectional fibrous media: a parallel computational approach *Phys. Fluids* **7** 2563–86
- [9] Happel J 1959 Viscous flow relative to arrays of cylinders *AIChE J.* **5** 174–7
- [10] Hasimoto H 1959 On the periodic fundamental solutions of the stokes equations and their application to viscous flow past a cubic array of spheres *J. Fluid Mech.* **5** 317–28
- [11] Higdon J J L and Ford G D 1996 Permeability of three-dimensional models of fibrous porous media *J. Fluid Mech.* **308** 341–61
- [12] Howells I D 1974 Drag due to the motion of a newtonian fluid through a sparse random array of small fixed rigid objects *J. Fluid Mech.* **64** 449–85
- [13] Jackson G W and James D F 1986 The permeability of fibrous porous media *Can. J. Chem. Eng.* **64** 364–74
- [14] Kuwabara S 1959 The forces experienced by randomly distributed parallel circular cylinders or spheres in a viscous flow at small reynolds numbers *J. Phys. Soc. Japan* **14** 527–32
- [15] Langmuir I 1942 Report of smokes and filters. part IV of a reports for the office of scientific research and development, OSRD, no. 865, ser. no 353 Rodebush *et al* 1942 Filtration of aerosols and development of filter materials *Technical Report*
- [16] Sangani A S and Acrivos A 1982 Slow flow past periodic arrays of cylinders with application to heat transfer *Int. J. Multiphase Flow* **8** 193–206
- [17] Sangani A S and Yao C 1988 Transport processes in random arrays of cylinders. II: Viscous flow *Phys. Fluids.* **31** 2435–44
- [18] Sparrow E M and Loeffler A L 1959 Longitudinal laminar flow between cylinders with application to heat transfer *AIChE J.* **5** 325–30
- [19] Spielman L and Goren S L L 1968 Model for predicting pressure drop and filtration efficiency in fibrous media *Environ. Sci. Technol.* **2** 279–87
- [20] Koponen A, Kandhai D, Hellen E, Alava M, Hoekstra A, Kataja M, Niskanen N, Sloom P and Timonen J 1998 Permeability of three-dimensional random fiber webs *Phys. Rev. Lett.* **80** 716–19
- [21] Yagushi Y, Hojo H, Lee D G and Kim E G 1995 Measurement of planar orientation of fibers for reinforced thermoplastic using image processing *Int. Polym. Process.* **3** 262–9
- [22] Xu J, Kim J, Ho T and Lee L 1993 *Polym. Composites* **14** 51–8
- [23] Skartsis L, Khomani B and Kardos J L 1992 Polymeric flow through fibrous media *J. Rheol.* **36** 589–620
- [24] Tripathi A and Chhabra R P 1992 Slow power-law fluid flow relative to an array of infinite cylinders *Ind. Eng. Chem. Res.* **31** 2754
- [25] Brusckhe M V and Advani S G 1993 Flow of generalized newtonian fluids across a periodic array of cylinders *J. Rheol.* **37** 479–98
- [26] Tripathi A and Chhabra R P 1996 Transverse laminar flow of non-newtonian fluids over a bank of cylinders *Chem. Eng. Commun.* **147** 197
- [27] Vijaysri M, Chhabra R P and Eswaran V 1999 Power-law fluid flow across an array of infinite circular cylinders: a numerical study *J. Non-Newtonian Fluid Mech.* **87** 263–82
- [28] Spelt P D M, Selerland T, Lawrence C J and Lee P D 2001 Drag coefficient for arrays of cylinders in flow of power-law fluids *Proc. 14th Australian Fluid Mech. Conf. (Adelaide University, Adelaide, Australia)* pp 881–4
- [29] Woods J K, Spelt P D M, Lee P D, Selerland T and Lawrence C J 2003 Creeping flows of power-law fluids through periodic arrays of elliptical cylinders *J. Non-Newtonian Fluid Mech.* **111** 211–28
- [30] Shah C B and Yortsos Y C 1995 Aspect of flow of power-law fluids in porous media *AIChE J.* **41** 1099–112
- [31] Bourgeat A and Mikelic A 1996 Homogenization of a polymer through a porous medium *Nonlinear Anal. Theory Meth. Appl.* **26** 1221–53
- [32] Auriault J-L, Royer P and Geindreau C 2002 Filtration law for power law fluids in anisotropic media *Int. J. Eng. Sci.* **40** 1151–63
- [33] Bensoussan A, Lions J-L and Papanicolaou G 1978 *Asymptotic Analysis for Periodic Structures* (Amsterdam: North-Holland)
- [34] Sanchez-Palencia E 1980 *Non-Homogeneous Media and Vibration Theory Lectures Notes in Physics* vol 127 (Berlin: Springer).
- [35] Auriault J-L 1991 Heterogeneous medium is an equivalent description possible? *Int. J. Eng. Sci.* **29** 785–95
- [36] Femlab 2002 Reference manual, version 2.3. [www.femlab.com](http://www.femlab.com)
- [37] Keller J B 1964 Viscous flow through a grating or lattice of cylinders *J. Fluid Mech.* **18** 94–6